Quantitative Analysis of Tyrosine Phosphorylation from FFPE Tissues Reveals Patient-Specific Signaling Networks

Ishwar N. Kohale[1,2,3], Danielle M. Burgenske[4], Ann C. Mladek[4], Katrina K. Bakken[4], Jenevieve Kuang[2,3], Judy C. Boughey[5], Liewei Wang[6], Jodi M. Carter[7], Eric B. Haura[8], Matthew P. Goetz[9], Jann N. Sarkaria[4], and Forest M. White[1,2,3]

ABSTRACT

Human tissue samples commonly preserved as formalin-fixed paraffin-embedded (FFPE) tissues after diagnostic or surgical procedures in the clinic represent an invaluable source of clinical specimens for in-depth characterization of signaling networks to assess therapeutic options. Tyrosine phosphorylation (pTyr) plays a fundamental role in cellular processes and is commonly dysregulated in cancer but has not been studied to date in FFPE samples. In addition, pTyr analysis that may otherwise inform therapeutic interventions for patients has been limited by the requirement for large amounts of frozen tissue. Here we describe a method for highly sensitive, quantitative analysis of pTyr signaling networks, with hundreds of sites quantified from one to two 10-μm sections of FFPE tissue specimens. A combination of optimized magnetic bead–based sample processing, optimized pTyr enrichment strategies, and tandem mass tag multiplexing enabled in-depth coverage of pTyr signaling networks from small amounts of input material. Phosphotyrosine profiles of flash-frozen and FFPE tissues derived from the same tumors suggested that FFPE tissues preserve pTyr signaling characteristics in patient-derived xenografts and archived clinical specimens. pTyr analysis of FFPE tissue sections from breast cancer tumors as well as lung cancer tumors highlighted patient-specific oncogenic driving kinases, indicating potential targeted therapies for each patient. These data suggest the capability for direct translational insight from pTyr analysis of small amounts of FFPE tumor tissue specimens.

Significance: This study reports a highly sensitive method utilizing FFPE tissues to identify dysregulated signaling networks in patient tumors, opening the door for direct translational insights from FFPE tumor tissue banks in hospitals.

Introduction

The rise of targeted therapeutics over the past two decades has highlighted a need for personalized cancer medicine to match optimal therapy to each patient. Precision medicine has commonly relied on genomic and transcriptomic tumor profiling (1, 2), yet these approaches have yielded limited success, possibly due to incomplete systems biology characterization of the tumors. While these "omics" approaches provide information on genomic mutations or altered transcript expression, neither approach directly measures signaling networks that drive tumor progression and regulate inherent and acquired therapeutic resistance. Analysis of phosphorylation-mediated signaling networks can provide crucial information on oncogenic drivers or dysregulated networks in patients (3).

Tyrosine phosphorylation (pTyr) accounts for only 0.1% to 1% of the total phosphoproteome, is highly conserved and tightly regulated, and controls many aspects of cellular and tumor biology (4, 5). Thirty percent of the known oncoproteins are tyrosine kinases (TK; ref. 6), and their disproportionate role in oncology has led to development of many TK inhibitors (TKI; ref. 7). Quantification of tyrosine phosphorylation can measure activated signaling networks in tumors and therefore highlight particular therapeutic options (8, 9). However, such analysis has historically been limited by the large amounts of clinical tissue required, and the need for frozen tissues, both of which can be challenging to obtain routinely.

Human tissue specimens obtained from diagnostic and surgical procedures are commonly preserved as formalin-fixed paraffin-embedded (FFPE) tissues in the clinic, and FFPE tissues are readily available in tumor tissue banks (10). While protein expression and global phosphorylation are increasingly being studied in FFPE tissues (11–14), global phosphorylation enrichment techniques typically yield few tyrosine phosphorylation sites due to its low abundance, typically <1% of the phosphoproteome (4). In addition, given previous reports of postsurgical ischemic effects on phosphorylation (15, 16), it is not known how well tyrosine phosphorylation is preserved in FFPE tissues. Therefore, a comparison of tyrosine phosphorylation signaling in FFPE and flash-frozen tissues is required to determine whether FFPE tissues can provide accurate quantification of cell signaling networks.

[1]Department of Biological Engineering, Massachusetts Institute of Technology, Cambridge, Massachusetts. [2]Koch Institute for Integrative Cancer Research, Massachusetts Institute of Technology, Cambridge, Massachusetts. [3]Center for Precision Cancer Medicine, Massachusetts Institute of Technology, Cambridge, Massachusetts. [4]Department of Radiation Oncology, Mayo Clinic, Rochester, Minnesota. [5]Department of Surgery, Mayo Clinic, Rochester, Minnesota. [6]Department of Molecular Pharmacology and Experimental Therapeutics, Mayo Clinic, Rochester, Minnesota. [7]Department of Laboratory Medicine and Pathology, Mayo Clinic, Rochester, Minnesota. [8]Department of Thoracic Oncology, H. Lee Moffitt Cancer Center and Research Institute, Tampa, Florida. [9]Department of Oncology, Mayo Clinic, Rochester, Minnesota.

Corresponding Author: Forest M. White, Department of Biological Engineering, Koch Institute for Integrative Cancer Research, Massachusetts Institute of Technology, 500 Main Street, 76-353, Cambridge, MA 02142. Phone: 617-258-8949; Fax: 617-258-0225; E-mail: fwhite@mit.edu

Cancer Res 2021;81:3930–41

doi: 10.1158/0008-5472.CAN-21-0214

We have developed an approach enabling tyrosine phosphorylation profiling of FFPE tissues with unprecedented sensitivity. We demonstrate quantification of approximately 2,000 pTyr sites belonging to critical cancer pathways from multiple 10-μm sections of FFPE tissues, representing an approximately 20-fold improvement in sensitivity for pTyr analysis. To understand the effects of FFPE preservation on pTyr levels, we compared pTyr profiles of flash-frozen and FFPE tissues derived from the same tumors and show that FFPE tissues faithfully preserve most, but not all, pTyr signaling. Using our optimized protocol, >900 pTyr sites were quantified from single-tissue punches obtained from clinical FFPE blocks containing breast cancer specimens, and from one or two 10-μm sections of FFPE from non–small cell lung cancer (NSCLC) patient tissues. Differential activation of oncogenic proteins such as EGFR, SRC, and MET was observed in different triple-negative breast cancer (TNBC) tumors, highlighting putative patient-specific oncogenic driving kinases for consideration of targeted therapeutic approaches. Finally, we quantify the effects of afatinib treatment on frozen and FFPE preserved EGFR-driven glioblastoma (GBM) tumors, demonstrating the potential for pTyr analysis to monitor therapeutic impact *in vivo*. Together, these results highlight the direct translational potential of pTyr analysis of FFPE tumor tissue specimens.

Materials and Methods

Animal studies

Studies involving animals were approved by the Institutional Animal Care and Use Committee at Mayo Clinic. The GBM6 patient-derived xenograft (PDX) cell line is maintained by serial heterotopic tumor passaging in mice at Mayo Clinic. The full genotypic and phenotypic characterization of GBM6 cell line is available at the Mayo Clinic PDX National Resource (17). The cells were authenticated by short tandem repeat analysis and were previously tested for *Mycoplasma* contamination. GBM6 cells were used at passage 1 after resecting from the mouse flank tumor. The cells were maintained in short-term explant cultures in FBS containing media prior to injection into the flank of athymic nude mice at a density of 2 million cells per animal (1:1 ratio of cells and Matrigel). Once tumors reached 200 to 250 mm^3 (∼14 days), animals were treated with 24 mg/kg of afatinib or vehicle control by oral gavage once daily for 3 days. Each animal received three doses, and tumors were harvested 2 hours after the last dose. Immediately after resection, half of the tumors were flash frozen in LN_2 and stored at −80°C, while formalin fixation was initiated on the other half of the tumor to process into FFPE blocks. Tumors were fixed in 10% formalin before being exposed to an ethanol gradient and xylene prior to embedding.

Clinical samples

All human FFPE and flash-frozen tissues were obtained in accordance with approved protocols. Breast cancer tissues were collected at Mayo Clinic (with Institutional Review Board approval) and lung cancer FFPE tissues were collected at Moffitt Cancer Center (#MCC18334). Detailed clinical and pathologic information about the clinical samples is provided in Supplementary Data.

FFPE protein extraction and lysis

Step-by-step detailed protocol for protein/peptide extraction from FFPE tissues is provided in Supplementary Data. Briefly, thin slices with 10-μm size were sectioned with microtome, and sections were collected in 1.7 mL microcentrifuge tubes. Sections were deparaffinized by washing with 500 μL xylene twice, and then hydrated with 500 μL of ethanol for 5 minutes. The sections were incubated at 90°C in lysis buffer consisting of 50% 2,2,2-trifluoroethanol (TFE) in 25 mmol/L ammonium bicarbonate at pH 8.5, 1× HALT Protease and Phosphatase Inhibitor Cocktail (Thermo Fisher Scientific) and 10 mmol/L of dithiothreitol (DTT) for 1 hour. Lysates were sonicated for 10 minutes. Thiols were alkylated with 55 mmol/L iodoacetamide (IAA) in dark at room temperature for 1 hour. Proteins were desalted using SP3 beads (Thermo Fisher Scientific) as described below.

Frozen tissue protein extraction

Frozen tumors were homogenized in ice-cold 8 mol/L urea supplemented with 1× HALT Protease and Phosphatase Inhibitor Cocktail. Frozen tumors were also lysed with a protocol similar to FFPE protein extraction where frozen tumors were incubated in lysis buffer containing 50% TFE in 25 mmol/L ammonium bicarbonate pH 8.5 and 1× HALT Protease and Phosphatase Inhibitor Cocktail at 90°C for 1 hour followed by homogenization. Protein concentrations were measured by bicinchoninic acid assay (BCA; Pierce) according to the manufacturer's instructions. Disulfide bonds were reduced with 10 mm DTT at 56°C for 1 hour followed by alkylation with 55 mmol/L IAA for 1 hour at room temperature in the dark.

Desalting and digestion with SP3 beads

After reduction and alkylation of proteins, lysates were incubated with sera-mag speed beads (SP3) and 50% ethanol for 8 minutes at room temperature. One mg of beads per 10-μm FFPE section and 10 μg of beads per 1 μg of protein from frozen tissues were used. Lysate-bead mix was incubated at magnetic rack for 2 minutes and supernatant was discarded. Beads were washed thrice with 200 μL of 80% ethanol. Proteins were digested for 18 to 24 hours on beads with sequencing grade trypsin (Promega) in 50 mmol/L HEPES buffer at 1:50 trypsin to protein ratio for frozen tumors and 2 μg trypsin per 10-μm section of FFPE. Peptides were collected in the supernatant by incubating beads on magnetic rack. Peptide concentrations were measured by BCA. Peptide aliquots were lyophilized and stored at −80°C.

Tandem mass tag labeling protocol

Peptides were labeled with TMT10plex or TMTpro16plex reagents (Thermo Fisher Scientific) in approximately 35 mmol/L HEPES and approximately 30% acetonitrile at pH 8.5 for 1 hour at room temperature at 1.5:4 peptide–to–tandem mass tag (TMT) reagent ratio (or higher). Labeling reactions were quenched with 0.3% of hydroxylamine. Samples were pooled, dried in speed-vac, and stored at −80°C.

Phosphopeptide enrichment

Immunoprecipitation (IP) and IMAC were used sequentially to enrich phosphotyrosine containing peptides. Label-free samples were resuspended in IP buffer (100 mmol/L Tris-HCl, 0.3% Nonidet P-40, pH 7.4) with 10 mmol/L imidazole. Samples were then incubated with TALON metal affinity resin beads (Takara) conjugated with 50 μg of Src SH2 domain (18) and 16 μg of Fab derived from 4G10 V312 variant (19). TMT-labeled samples were incubated in IP buffer consisting of 1% Nonidet P-40 with protein G agarose beads conjugated to 24 μg of 4G10 V312 IgG and 6 μg of PT-66 (Sigma) overnight at 4°C. Peptides were eluted twice, each with 25 μL of 0.2% trifluoroacetic acid for 10 minutes at room temperature followed by Fe-NTA spin column based IMAC enrichment.

High-Select Fe-NTA enrichment kit (Pierce) was used according to manufacturer's instructions with following modifications. Eluted peptides from IP were incubated with Fe-NTA beads containing 25 μL of

binding washing buffer for 30 minutes. Peptides were eluted twice with 20 μL of elution buffer into a 1.7 mL microcentrifuge tube. Eluates were concentrated in speed-vac until 1 to 5 μL of sample remained, and then resuspended in 10 μL of 5% acetonitrile in 0.1% formic acid. Samples were loaded directly onto an in-house packed analytic capillary column [50 μm inner diameter (ID) × 10 cm] packed with 5 μm C18 beads (YMC gel, ODS-AQ, AQ12S05).

LC/MS-MS analysis

LC/MS-MS of pTyr peptides were carried out on an Agilent 1260 LC coupled to a Q Exactive HF-X mass spectrometer (Thermo Fisher Scientific). Peptides were separated using a 140-minute gradient with 70% acetonitrile in 0.2 mol/L acetic acid at flow rate of 0.2 mL/minute with approximate split flow at 20 nL/minute. The mass spectrometer was operated in data-dependent acquisition with following settings for MS1 scans: m/z range: 350 to 2,000; resolution: 60,000; AGC target: 3×10^6; maximum injection time (maxIT): 50 ms. The top 15 abundant ions were isolated and fragmented by higher energy collision dissociation with following settings: resolution: 60,000; AGC target: 1×10^5; maxIT: 350 ms; isolation width: 0.4 m/z, collisional energy (CE): 33% for TMT labeled and 29% for label free, dynamic exclusion: 20 seconds. For a global phosphoproteomic and proteomic analysis, half of the supernatants from pTyr IPs were fractionated into 10 fractions as described previously (20). One tenth of each fraction was analyzed to quantify protein levels, while rest of the fraction was enriched for phosphopeptides using High-Select Fe-NTA enrichment kit. LC/MS-MS of fractionated samples was performed on an Easy-nLC 1000 coupled to a Q Exactive HF-X mass spectrometer. Peptides were eluted with 80% acetonitrile in 0.1% formic acid using a 90-minute gradient. Instrument settings were similar to that of pTyr analysis except top 10 most abundant ions were isolated and fragmented with CE of 29% and maxIT of 150 ms.

Crude peptide analysis was performed on a Q Exactive Plus mass spectrometer to correct for small variation in peptide loadings for each of the TMT channels. Approximately 30 ng of the supernatant from pTyr IP was loaded onto an in-house packed precolumn (100 μm ID × 10 cm) packed with 10 μm C18 beads (YMC gel, ODS-A, AA12S11) and analyzed with a 70-minute LC gradient. MS1 scans were performed at following settings: m/z range: 350 to 2,000; resolution: 70,000; AGC target: 3×10^6; maxIT: 50 ms. The top 10 abundant ions were isolated and fragmented with CE of 33% at a resolution of 35,000.

Peptide identification and quantification

Mass spectra were processed with Proteome Discoverer version 2.2 (Thermo Fisher Scientific, RRID:SCR_014477) and searched against the human SwissProt database using Mascot version 2.4 (Matrix Science, RRID:SCR_014322). MS-MS spectra were searched with mass tolerance of 10 ppm for precursor ions and 20 mmu for fragment ions. Cysteine carbamidomethylation, TMT-labeled lysine, and TMT-labeled peptide N-termini were set as fixed modifications. Oxidation of methionine and phosphorylation of serine, threonine and tyrosine were searched as dynamic modifications. TMT reporter quantification was extracted and isotope corrected in Proteome Discoverer. Peptide spectrum matches (PSM) were filtered according to following parameters: rank = 1, search engine rank = 1, mascot ion score > 15, isolation interference < 30%, average TMT signal > 1,000. Peptides with missing values across any channel for PDX tumor analysis were filtered out. Phosphorylation sites were localized with ptmRS module (21) with 216.04 added as a diagnostic mass for pTyr immonium ion (22). PSMs with >95% localization probability for all phosphorylation sites were included for further analysis. For global proteome analysis, peptides were additionally filtered with FDR (Percolator q-value) < 0.01. Only proteins with either two unique peptides or two PSMs were quantified for downstream proteomic analysis.

Data analysis

Data analyses were performed in Python (version 3.6) and Microsoft Excel 2016. TMT reporter ion intensities from PSMs were summed for each unique phosphopeptide. For protein level quantification, TMT reporter intensities were summed for all unique peptides. Peptide or protein quantification were normalized with relative median values obtained from crude lysate analysis to adjust for sample loading in TMT channels. Student t test was used to determine statistical significance between treatment groups. Unsupervised hierarchical clustering was performed on the basis of Pearson correlation distance metric, unless otherwise specified. Protein networks were obtained from STRING (version 11.0) database (23) and visualized using the Cytoscape platform (version 3.8, RRID:SCR_003032; ref. 24). Gene ontology and Kyoto Encyclopedia of Genes and Genomes (KEGG) pathway enrichment were performed using STRING (RRID:SCR_005223) and PANTHER (version 15.0, RRID:SCR_004869; ref. 25) databases. Kinome trees were obtained from KinMap (26) with illustration reproduced courtesy of Cell Signaling Technology, Inc (www.cellsignal.com). For cluster set enrichment analysis, pTyr sites were rank ordered according to their mean normalized phosphorylation levels compared to all nine tumors, and running enrichment score (ES) was calculated (27). Significance (P) of ES was derived from 1,000 permutations where ranks of pTyr sites were randomized. P represents fraction of permutations where the maximum ES was greater than the observed one.

Data availability

The mass spectrometry (MS) proteomics data have been deposited to the ProteomeXchange Consortium via the PRIDE (28) partner repository with the dataset identifier PXD020284 and 10.6019/PXD020284. Information on mass spec raw files and TMT labeling strategy is detailed in Supplementary Table S1. All other data are available upon request.

Results

Phosphotyrosine analysis of FFPE samples is feasible and provides quantitative data on underlying biology

We set out to develop a method for the quantitative characterization of pTyr signaling networks from small amounts of FFPE tissues, and to determine whether the signaling networks quantified from these tissue specimens could provide relevant biological insights. To this end, we developed a protocol combining TFE-based protein extraction (13) with paramagnetic SP3 bead–based sample processing (11, 12) that allows for robust and sensitive phosphoproteomic analysis of FFPE tissues (**Fig. 1A**). This optimized protocol led to peptide yields of approximately 2 μg per mm^2 of a 10-μm section of FFPE tissue or roughly 200 μg peptides for a 10 mm × 10 mm × 10 μm section, and scales with larger tissue sections of FFPE blocks (Adj $R^2 = 0.95$; Supplementary Fig. S1A). To assess the feasibility of quantifying pTyr signaling in FFPE tissues, we enriched pTyr-containing peptides through a two-step protocol, using anti-pTyr antibodies for IP and immobilized metal affinity chromatography (IMAC) to remove nonspecifically retained nonphosphorylated peptides prior to analysis by LC/MS-MS (29). Using this platform, we performed MS analysis of enriched pTyr peptides from 12 10-μm sections from PDX GBM

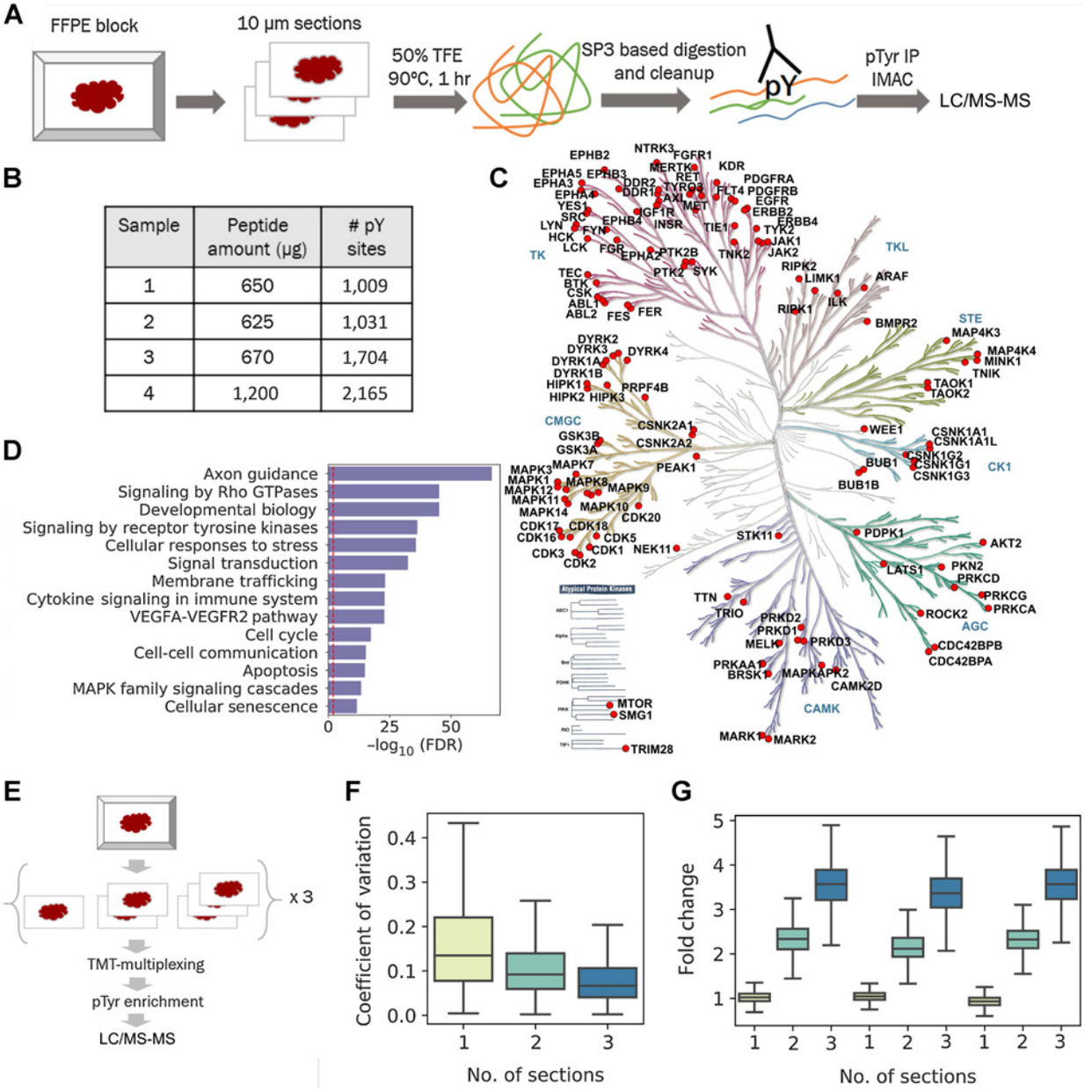

Figure 1.

Phosphotyrosine analysis from 10-µm sections of FFPE tissues. **A,** Optimized workflow for extraction and digestion of proteins from FFPE tissues followed by two-step enrichment of pTyr peptides for LC/MS-MS analysis. **B,** Number of pTyr sites identified from multiple 10-µm sections of GBM6 PDX tumors. **C,** Kinome tree depicting pTyr-containing proteins identified in PDX tumors. **D,** Selected reactome pathways enriched in gene ontology analysis of pTyr proteins. Dashed red line depicts FDR = 0.01. **E,** Schematic workflow for a multiplexed pTyr analysis of one, two, or three 10-µm sections of FFPE tissues in triplicate. **F,** CV observed across multiple sections of FFPE tissues ($n = 3$ replicates). Median CV for one, two, or three sections was 13.5%, 9.2%, and 6.7%, respectively. **G,** Fold change of TMT intensities of peptides quantified in each channel compared with the average of TMT intensities from single sections on a peptide basis. Error bars represent interquartile range.

Sample	Peptide amount (µg)	# pY sites
1	650	1,009
2	625	1,031
3	670	1,704
4	1,200	2,165

tumors (GBM6; ref. 30). This approach led to identification of 1009, 1031, 1704 and 2165 pTyr sites in four different GBM6 tumors (**Fig. 1B**; Supplementary Tables S2–S5), including pTyr sites on 129 kinases spanning across multiple branches of the kinome tree (**Fig. 1C**). Gene ontology analysis of pTyr proteins indicated enrichment of multiple reactome pathways including axon guidance, signaling by Rho GTPases, signaling by receptor tyrosine kinases (RTK), cell cycle, and cellular senescence, providing further evidence that pTyr enrichment and analysis yields insight into activated cellular pathways in tumors (**Fig. 1D**).

Routine pTyr and global phosphoproteomic analysis of clinical specimens has been hampered by the amount of tissue samples required for such experiments. To assess the low-input sample sensitivity and robustness of our FFPE pTyr analysis platform, peptides

derived from one, two, or three 10-μm thick sections of FFPE tissue, corresponding to approximately 50, 100, or 150 μg of peptides per sample, were labeled with TMT for multiplexing (**Fig. 1E**) prior to pTyr enrichment and LC/MS-MS analysis. This approach led to identification and quantification of 816 pTyr containing peptides in each sample (Supplementary Table S6). Median coefficient of variation (CV) for peptides quantified across the replicates were 13.5%, 9.2%, and 6.7% for one, two, or three sections, respectively, suggesting robust quantification even with a single 10-μm section (**Fig. 1F**). Median fold change compared with average of single sections for peptides within the same samples were 1.02, 2.32, and 3.57 for one, two, or three sections (**Fig. 1G**), respectively. Similar relative quantification was also observed for non-phosphopeptides quantified from the supernatant of pTyr IP, suggesting that sample processing of single sections leads to increased sample loss due to the small amount of input material (Supplementary Fig. S1B; Supplementary Table S7). Quantified phosphoproteins were enriched in RTKs as well as other branches in the kinome tree (Supplementary Fig. S1C), and belong to multiple pathways such as EGFR, FGFR, and PI3K signaling, many of which have been already implicated in promoting GBM tumor progression and therapeutic resistance (Supplementary Fig. S1D; refs. 31–33). Overall, these data suggest that pTyr analysis of a single 10-μm section of FFPE-preserved tissue specimen is feasible and can yield hundreds of pTyr peptides representing a broad swath of GBM tumor biology.

pTyr analysis of NSCLC FFPE clinical tissue sections

Next, we performed pTyr analysis on FFPE clinical samples obtained from a lung cancer tumor tissue bank to assess low-input sample feasibility of our method. In addition, we wanted to determine whether pTyr analysis of FFPE lung cancer tumor tissues could reveal information regarding EGFR phosphorylation and activation. We collected FFPE tissues from 9 patients with NSCLC that had mutations in EGFR (**Fig. 2A**). Two 10-μm sections were obtained from each tissue specimen, and proteins were extracted and digested to peptides following our FFPE protocol. We obtained peptide yields ranging from 157 to 595 μg from each patient, suggesting that a single 10-μm section would have sufficed for pTyr analysis for most of the patients (Supplementary Fig. S2A). MS-MS analysis of enriched pTyr peptides led to identification of 962 sites (Supplementary Table S8), including 70 kinases spanning across multiple kinase families, including Erbbs (EGFR, ERBB2, ERBB3), focal adhesion kinases (PTK2, PTK2B, PTK6), and MAPKs (MAPK 1, 3, 7, 9, 11–14; Supplementary Fig. S2B). Because tumor tissues were collected from patients with EGFR mutations, we first quantified pTyr levels on EGFR to examine any correlation between the genomic mutations and phosphorylation/activation of EGFR. Genomic mutations were not correlated with EGFR phosphorylation. For instance, patient 4 (P4), P7, and P9 all had L858R mutation; however, P7 and P9 had approximately 2-fold and approximately 10-fold higher EGFR phosphorylation compared with P4, respectively (**Fig. 2B**; Supplementary Fig. S2C–S2E).

To identify activated signaling networks in each tumor and extract coregulated sites, we performed hierarchical clustering on the co-correlation matrix for individual pTyr sites. This co-correlation and clustering analysis revealed three main clusters (**Fig. 2C**; Supplementary Table S8): Cluster 1 was highly enriched in innate and adaptive immune signaling, including Fc epsilon RI and T-cell receptor signaling pathway consisting of a well-characterized network including proteins such as T-cell receptor (CD247, CD3D, CD3E, CD3G), ZAP70 and LCK (**Fig. 2D** and **E**), whereas cluster 2 was mainly enriched in focal adhesions and regulation of actin cytoskeleton pathways consisting of proteins such as RHOA, ROCK2, and ITGB1 (Supplementary Fig. S2F and S2G), and phosphoproteins in cluster 3 consisted of several ribosomal proteins as well splicing factors (Supplementary Fig. S2H and S2I). To identify patients with these differentially activated signaling networks, we performed enrichment analysis (27) for each cluster in each patient. Cluster 1 was enriched in P6, P8, and P9, suggesting immune infiltration and activation in these tumors, which also featured high phosphorylation levels of many other RTKs (**Fig. 2F;** Supplementary Fig. S3A and S3B). Interestingly, cluster 2 and cluster 3 were highly enriched in single patients, P1 and P2, respectively, suggesting that these tumors may be driven, in part, by splicing and ribosomal dysregulation and integrin/focal adhesion signaling (Supplementary Fig. S3C and S3D). Together, these data suggest that EGFR mutation status may be a poor predictor of EGFR phosphorylation and activation, as has been suggested previously (34). These findings also highlight the potential for potential translational insight from pTyr analysis of one to two 10-μm sections from FFPE tumor tissue specimens.

Phosphotyrosine signaling is preserved in clinical specimens

Our initial data indicate that analyses of pTyr signaling in FFPE GBM PDX tumors and FFPE tumors from patients with NSCLC can yield a large number of identified and quantified pTyr peptides. However, there was some concern that the time required for formalin fixation, which occurs at approximately 1 mm/hour (35), may lead to altered signaling compared with the time required for flash freezing, which occurs on the subsecond/second timescale, especially given previous data suggesting that ischemia alters pTyr signaling within minutes after resection (15, 16). Therefore, we wanted to assess whether pTyr signaling in FFPE tissues is similar to concomitantly obtained frozen tissues in a clinical setting. Thus, we performed a comparison analysis on clinical specimens derived from the Mayo Clinic Breast Cancer SPORE tissue registry where matched frozen and FFPE specimens are collected prospectively. We obtained 20 breast cancer tissue specimens, including 10 tumor samples wherein FFPE tissue blocks and matched flash-frozen tumor samples were harvested in parallel from the same tumors (**Fig. 3A**). Two-millimeter punches of tumor-rich regions from the FFPE tissue blocks were obtained by pathologists. Tumor-rich content was verified in the flash-frozen optimal cutting temperature–embedded tissues by pathologist evaluation of hematoxylin and eosin–stained cryosections. Proteins were extracted from each tissue type with the corresponding workflows, digested to peptides, and labeled with isobaric mass tags (TMT10plex). Analysis of enriched pTyr peptides led to identification and quantification of 927 and 382 sites in FFPE and frozen tissues (Supplementary Tables S9 and S10), respectively, with 281 sites quantified across both sets of analyses. We did not observe any correlation of pTyr levels with storage time of FFPE tissues (Supplementary Fig. S4A and S4B). Peptides containing pTyr sites from both analyses clustered by patient (**Fig. 3B**), and the average Pearson correlation coefficient between FFPE and frozen pairs ($R = 0.51 \pm 0.18$) was significantly higher than that of all other pairwise analyses ($R = 0.05 \pm 0.16$, $P = 7.56 \times 10^{-17}$; **Fig. 3C**), indicating that similarity between frozen and FFPE tissues outweighed interpatient heterogeneity. Despite their relative similarity, the heatmap and correlation coefficients both highlight that FFPE and frozen tumor pairs are not identical. To gain insight into the signaling components that were most highly preserved during FFPE storage, we extracted the sites that had highest correlation between the FFPE and frozen samples. Intriguingly, the top 30 most highly correlated sites belonged to proteins such as EGFR, MAPKs, STATs, and PI3Ks, many of which are essential nodes in cellular signaling pathways, highlighting that FFPE tissues and frozen tissues

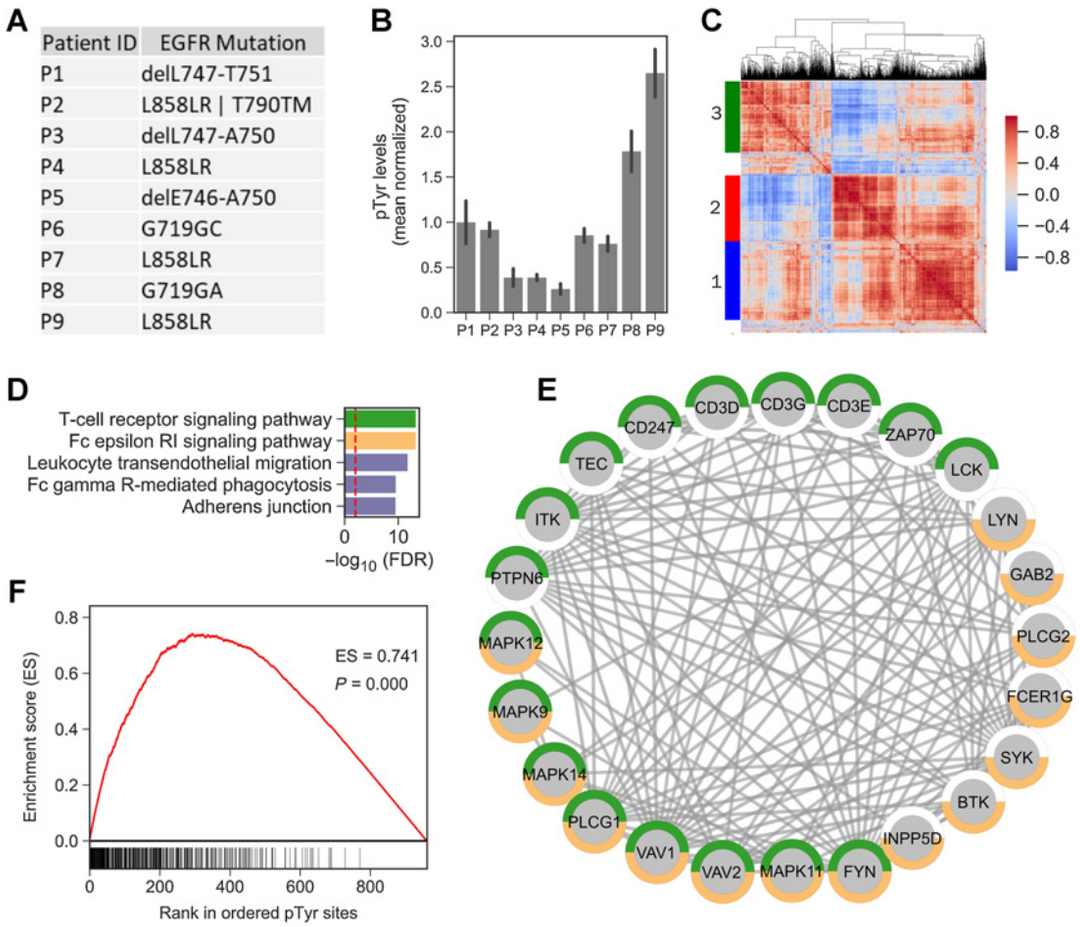

Figure 2.

Phosphotyrosine analysis of archived FFPE tissues from patients with NSCLC. **A,** Mutation status of EGFR in various patients. **B,** Phosphotyrosine levels of EGFR averaged across multiple tyrosine sites (Y1068, Y1148, and Y1173) plotted relative to the mean of all nine tumors. Error bars, SD. **C,** Hierarchical clustering heatmap of co-correlation matrix for pTyr sites quantified in NSCLC FFPE specimens. Clustering was based on Euclidean distance. Color scale represents Pearson correlation. Three main clusters were identified in this analysis. **D,** Top five significantly enriched KEGG pathways in pTyr proteins belonging to cluster 1. Dashed red line depicts FDR q-value = 0.01. **E,** Interaction network of proteins belonging to T-cell receptor (green) and Fc epsilon RI (orange) signaling pathways that were identified in cluster 1. All of the interactions are highest confidence based on all interaction sources except text mining from STRING database. **F,** Cluster set enrichment analysis for cluster 1 pTyr sites in P9.

provide similar information on dysregulated biological networks in the clinic (**Fig. 3D**; Supplementary Fig. S4C–S4H; Supplementary Table S11). Many of the least correlated sites belonged to proteins involved in immune regulation and cytoskeletal organization, potentially highlighting dissimilarity between the tumor-rich and stromal regions because FFPE tissues were punched from tumor-rich regions, while the frozen tissue specimens were not necessarily tumor enriched given the larger size of tissue (Supplementary Fig. S4I).

Patients with TNBC have poor prognosis and few therapeutic options beyond chemotherapy. Protein targets such as ERBBs, MET, SRC, MAPKs, and STATs have been explored as potential therapeutic targets for breast cancer (36); therefore, we wanted to assess the phosphorylation state of these proteins across the 10 FFPE clinical tumor specimens. Of the 10 tumors, six were classified as estrogen receptor positive/progesterone receptor positive, three were classified as triple negative (P1, P2, and P5), and one was functionally similar to TNBC (P8) based on previous IHC analysis (Supplementary Data). To quantify phosphorylation, we averaged multiple pTyr sites for each interesting protein target and plotted values relative to the mean of all 10 tumors (**Fig. 3E**). This analysis led to identification of differential activation of proteins in different patients. For instance, P1 had high relative phosphorylation of EGFR, whereas P3 had high relative phosphorylation of ERBB3. In contrast, P8 had high relative phosphorylation for all ERBB family members in addition to PDGFRB, SRC, and PI3KR2, suggesting multiple potential drivers, or potentially a more heterogeneous tumor. MET was highly upregulated in P2 and P5. This differential phosphorylation of protein targets highlights potential patient-specific oncogenic driving kinases, and may indicate the potential benefit of an individualized targeted therapeutic approach for each patient. For instance, an EGFR inhibitor is more likely to have a therapeutic effect only in P1, but not in other patients based on this analysis. We also discovered evidence of T-cell immune infiltration and activation in P5 and P6 as assessed by high phosphorylation on the T-cell receptor (CD247), suggesting a potential role for an immune checkpoint inhibitor in these patients. We observed high phosphorylation levels of same oncogenes in respective patients using

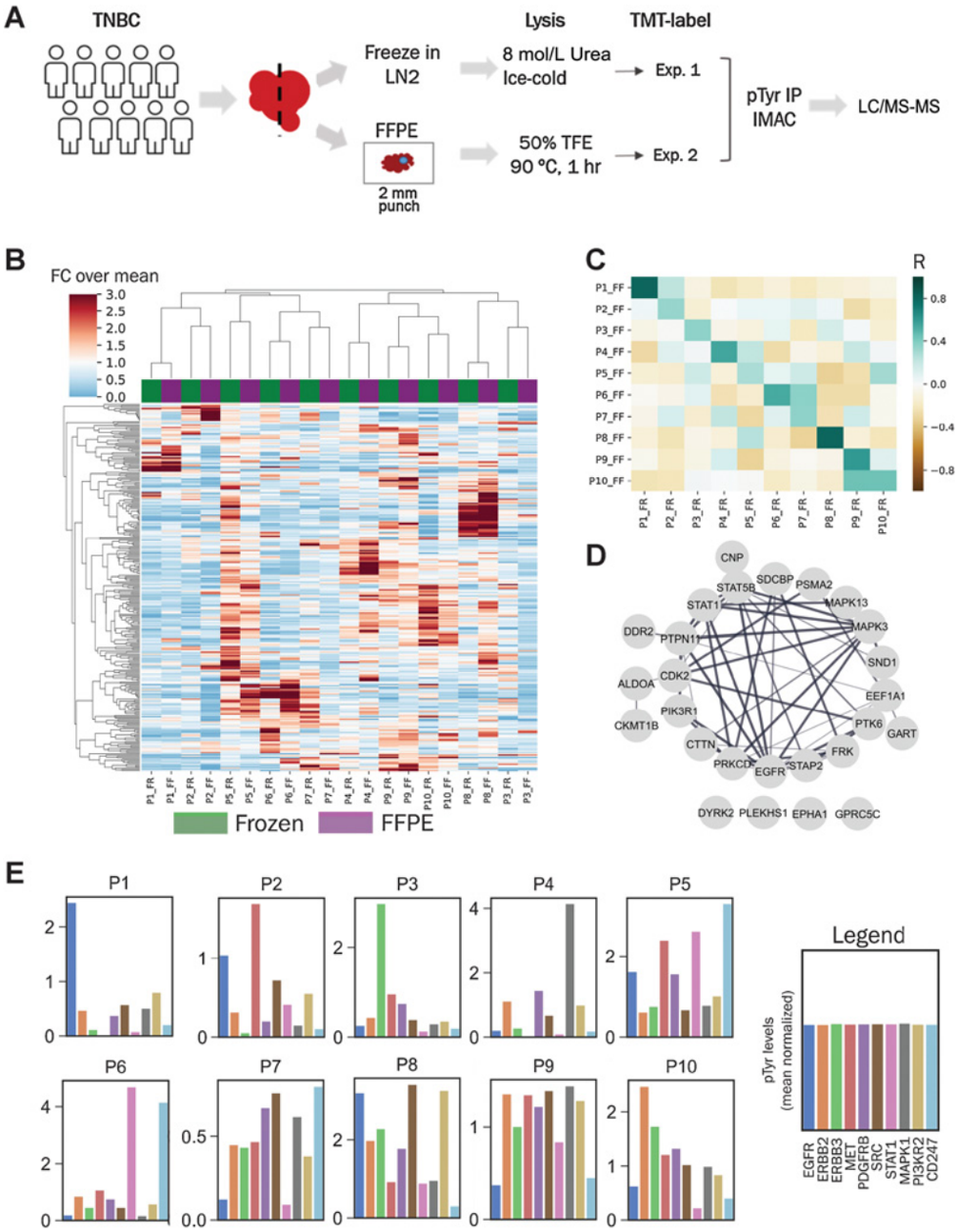

Figure 3.

Phosphotyrosine analysis of breast cancer clinical specimens. **A,** Experimental workflow to compare pTyr signaling in FFPE and flash-frozen specimens from breast cancer patient tumors. **B,** Hierarchical clustering heatmap based on Pearson correlation distance metric of pTyr peptides identified and quantified in FFPE and flash-frozen conditions. Quantification levels were mean normalized within each workflow before concatenating together. A total of 281 pTyr peptides were quantified in both workflows. FC, fold change. **C,** Heatmap of Pearson correlation (*R*) between flash-frozen and FFPE tissues for each patient. Average *R* for FFPE and frozen pairs (from same patient) was 0.51 ± 0.18 and 0.05 ± 0.16 for all other pairwise analyses. **D,** Interaction network of pTyr proteins that were highly preserved in FFPE tissues. Phosphotyrosine sites belonging to these proteins had highest Pearson correlation for quantified levels in flash-frozen and FFPE specimens. **E,** Barplots with phosphorylation levels of various proteins quantified for each patient based on FFPE tissues. Phosphorylation levels represent average phosphorylation across multiple pTyr sites for a given protein target and are plotted relative to the mean of all 10 tumors (mean normalized).

the frozen tumors (Supplementary Fig. S5). Overall, the comparative pTyr analysis of FFPE and frozen tissues from patients with breast cancer suggest that FFPE tissues may provide biologically meaningful information similar to frozen tissues in the clinic.

Comparison of pTyr, pSer/thr, and protein levels in FFPE and flash-frozen tissues after treatment with TKI

While pTyr analysis of FFPE tumors from patients with NSCLC and breast cancer showed various activated kinases in different patients, we

wanted to test whether the findings from FFPE tumors could be more broadly used for diagnostic purposes in the clinic. Analysis of GBM6 PDX tumors showed phosphorylation of various proteins including RTKs (**Fig. 1**). We extracted the 20 most abundant phosphopeptides belonging to RTKs to determine whether GBM6 tumors were driven by a specific RTK. As shown in **Fig. 4A**, the three most abundant, as well as 11 of the top 20, phosphopeptides belonged to EGFR. Well characterized sites such as Y845, Y1148, and Y1173 that have been positively associated with EGFR activation were highly phosphorylated, suggesting that GBM6 tumors are driven by EGFR, corroborating a previous study where GBM6 was found to have EGFRvIII amplification (30). Next, we treated GBM6 PDX tumors *in vivo* with afatinib, a second-generation EGFR inhibitor, or vehicle, to (i) determine whether PDXs would respond to EGFR inhibition as predicted from the pTyr analysis, (ii) determine whether our method can be broadly used in the clinic to measure therapeutic response, and (iii) understand the effect of FFPE preservation on pTyr signaling in a controlled setting. After resection, half of the tumor was flash frozen in liquid nitrogen, and other half was processed into an FFPE block (**Fig. 4B**). A piece of each flash-frozen tumor tissue was homogenized in 8 mol/L urea lysis buffer, as per our standard protocol (15, 37–39). FFPE tissues were lysed in 50% TFE at 90°C according to the FFPE protocol described above. To control for the effects of the FFPE protein extraction protocol, a separate aliquot of flash-frozen tissue was lysed

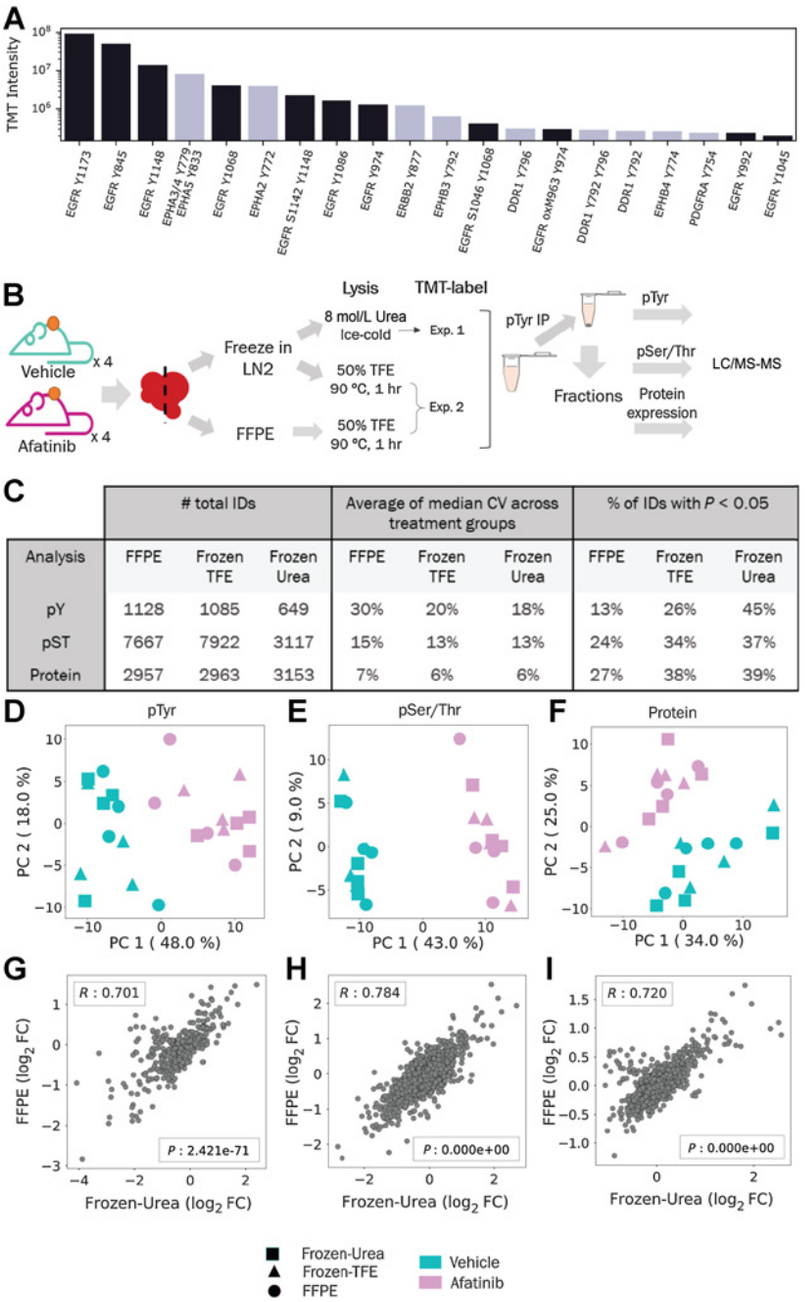

	# total IDs			Average of median CV across treatment groups			% of IDs with $P < 0.05$		
Analysis	FFPE	Frozen TFE	Frozen Urea	FFPE	Frozen TFE	Frozen Urea	FFPE	Frozen TFE	Frozen Urea
pY	1128	1085	649	30%	20%	18%	13%	26%	45%
pST	7667	7922	3117	15%	13%	13%	24%	34%	37%
Protein	2957	2963	3153	7%	6%	6%	27%	38%	39%

Figure 4.

Comparison of pTyr, pSer/Thr, and protein levels in FFPE and flash-frozen tissues after treatment with afatinib. **A,** TMT intensities of the 20 most abundant phosphopeptides belonging to RTKs from FFPE GBM6 PDX tumor from **Fig. 1E**. TMT values were summed across all channels and plotted for each phosphopeptide. **B,** Schematic of experimental design to compare proteomics in FFPE and flash-frozen tissues. **C,** Number of unique phosphopeptides or proteins identified and quantified across different workflows with observed CVs and proportion of significantly different IDs between vehicle and afatinib treatments ($n = 4$ biological replicates). **D–F,** PCA of phosphopeptides or proteins quantified across FFPE, Frozen-Urea, and Frozen-TFE workflows: pTyr ($n = 475$ peptides; **D**), pSer/Thr ($n = 2{,}283$ peptides; **E**), and protein ($n = 2{,}647$ proteins; **F**) levels. Quantified levels were mean normalized and $\log_2$ transformed within each workflow before concatenating together. **G–I,** Correlation plots of fold changes (FC) observed between afatinib- and vehicle-treated groups in Frozen-Urea samples and their FFPE pairs: pTyr (**G**), pSer/Thr (**H**), and proteins (**I**). For each phosphopeptide or protein, fold changes were calculated between mean levels observed in groups treated with afatinib ($n = 4$) and vehicle ($n = 4$). *R* represents Pearson correlation.

according to the FFPE protocol. Proteins extracted from these three protocols: (i) FFPE, (ii) flash frozen lysed in hot TFE (hereafter referred as Frozen-TFE), and (iii) flash frozen with standard 8 mol/L urea lysis (Frozen-Urea) were digested to peptides, labeled with 16-plex isobaric mass tags (TMTpro), enriched for pTyr, and analyzed by LC/MS-MS. The supernatant from the pTyr IP was fractionated and analyzed to assess the effect of FFPE preservation on global phosphorylation, for example, pSer/pThr, and protein expression. Analysis of pTyr signaling led to identification and quantification of 1128, 1085, and 649 peptides in FFPE, Frozen-TFE, and Frozen-Urea workflows, respectively (**Fig. 4C**; Supplementary Tables S12–S20). Fewer pTyr sites were identified in the Frozen-Urea condition, as only eight samples were multiplexed together in this analysis as opposed to 16 samples in the FFPE and Frozen-TFE analysis. Peptides derived from the Frozen-Urea workflow had CV of 18% across biological replicates, whereas Frozen-TFE and FFPE workflows had 20% and 30%, respectively, indicating that FFPE preservation may lead to increased variability among samples. We assessed the statistical significance of pTyr-peptides affected by afatinib treatment in each condition and found that 45% of the pTyr-peptides were statistically significantly different between vehicle- and afatinib-treated groups in the Frozen-Urea condition compared with 26% in Frozen-TFE and 13% in FFPE. Although samples clustered by treatment condition [afatinib vs. vehicle (Supplementary Fig. S6A)], there were some marked differences between FFPE and frozen tissues. Within each treatment condition, frozen pairs (TFE and Urea) derived from the same tumor tended to cluster together, while FFPE counterparts either clustered with each other or clustered with larger subclusters. Similarly, correlation between frozen pairs (0.72 ± 0.15) was statistically significantly higher than that of between FFPE and Frozen-TFE (0.46 ± 0.22, $P = 0.02$), suggesting that pTyr underwent minimal changes during protein extraction steps but more pronounced changes during FFPE preservation (Supplementary Table S21). Many of the sites that were at least 2-fold different between Frozen-Urea and FFPE conditions belonged to EGFR, GAB1, SPRY4, and MAPK1, suggesting that these sites are likely sensitive to FFPE processing–related changes (Supplementary Table S22). These results suggest that some changes in pTyr signaling can occur during FFPE preservation and that these changes can affect our confidence in determining signaling network changes due to drug treatment. In contrast to the pTyr data, pSer/Thr data and protein expression data still clustered by treatment condition, but not by preservation or processing technique (Supplementary Fig. S6B and S6C), suggesting that these peptides were less affected by sample preservation or processing, in agreement with previous studies (16). Despite similar CVs, the percentage of peptides that were statistically significantly different in the vehicle versus afatinib conditions were still lower in FFPE tissues (**Fig. 4C**), possibly because of overall lower TMT intensities for pSer/pThr and unmodified peptides derived from FFPE tissues (Supplementary Fig. S6D and S6E). Unexpectedly, pTyr-peptide intensities were higher in samples derived from FFPE tissues compared with Frozen-TFE (Supplementary Fig. S6F).

To further assess the effects of sample preservation and processing on signaling and proteomic analysis, we performed principal component analysis (PCA) on peptides or proteins that were quantified across all three workflows. PCA showed that despite different tissue preservation and processing methods pTyr, pSer/Thr, and protein levels segregated according to afatinib treatment (**Fig. 4D–F**). We also looked at the correlation between different preservation and processing methods on a peptide-specific basis. Average fold change of treated over the control samples were highly correlated between Frozen-Urea and FFPE tissues with R of 0.70, 0.78, and 0.72 for pTyr, pSer/Thr, and protein levels, respectively, underscoring that FFPE tissues preserve similar biology relative to frozen tissues (**Fig. 4G–I**). Taken together, these data suggest that pTyr signaling in FFPE tissues was comparable, but not identical, to the frozen tissues, as some changes in pTyr signaling occur during formalin fixation.

Effects of afatinib inhibition of the EGFR network are detectable in FFPE and frozen tissues

Given some differences in pTyr signaling during FFPE preservation, we wanted to understand whether FFPE tissues can still provide similar biological network information regarding the effect of afatinib treatment compared with frozen tissues. Treatment with afatinib is expected to lead to decreased EGFR activation; accordingly, we detected decreased tyrosine phosphorylation on several proteins in the EGFR pathway including EGFR itself, as well as sites on GAB1, GAB3, SHC1, SHC4, PTPN11 (SHP2), MAPK1 (ERK2), and MAPK3 (ERK1), all of which decreased by 2-fold to 10-fold in afatinib-treated tumors compared with vehicle control (**Fig. 5A**). In addition, other proteins directly downstream of EGFR such as CBL (endocytosis), PLCG1 (phospholipase c pathway), PIK3R2 (cell survival), and STAT5A/B (JAK–STAT pathway) also had downregulated pTyr levels in afatinib-treated tumors. Although effects of afatinib treatment could be read out with both frozen and FFPE tissues, downregulation of EGFR pathway was more prominent, in terms of fold change and reproducibility across different tumors, in frozen tissues compared with FFPE counterparts. Indeed, two of the afatinib-treated tumors preserved as FFPE even had higher pTyr levels in EGFR and GAB1 compared with their frozen pairs or the vehicle control. Altered signaling in these FFPE tumors was not due to the protein extraction step because frozen tissues processed with FFPE workflow (Frozen-TFE) did not exhibit such strong differences (Supplementary Fig. S7).

Although afatinib led to downregulation of pTyr signaling in EGFR pathway, it led to upregulation of EGFR and GAB1 at protein level (**Fig. 5A**), highlighting a potential therapeutic resistance pathway where tumor cells upregulate the protein target to overcome loss of activation. In addition, in response to afatinib, tumors exhibited higher pTyr levels in epithelial discoidin domain containing receptor 1 (DDR1), the non-receptor protein tyrosine kinase Src, and multiple Src-family kinase substrates (**Fig. 5B**), in agreement with previous work demonstrating Src and Src-family kinases (SFK) as a resistance mechanism for EGFR inhibition (38, 40). Phosphoproteins with increased pTyr levels in response to afatinib formed a strong interaction network associated with RTK signaling and locomotion pathways (**Fig. 5C**). These adaptive resistance pathways could be read out from frozen tissues and their FFPE counterparts, suggesting that, despite some signaling alterations during preservation, pTyr analysis of FFPE tissues can provide similar biological information compared with their frozen counterparts. Taken together, pTyr analysis of FFPE GBM6 tumors led to identification of EGFR as a potential driver of growth in GBM6 tumors, and treatment with afatinib led to downregulation of EGFR pathway, altogether suggesting that pTyr analysis of FFPE tissues can be used for both diagnostic purposes in identifying activated kinases as well as measuring therapeutic response after treatment in the clinic.

Discussion

FFPE tissues are widely available in the clinic and represent a rich resource to study molecular mechanisms of various diseases directly in patient specimens. Although MS-based proteomics methods have been increasingly used for FFPE samples, these studies have been limited to protein expression and global phosphorylation profiling, both of which are present in high abundance in cells. Identification and

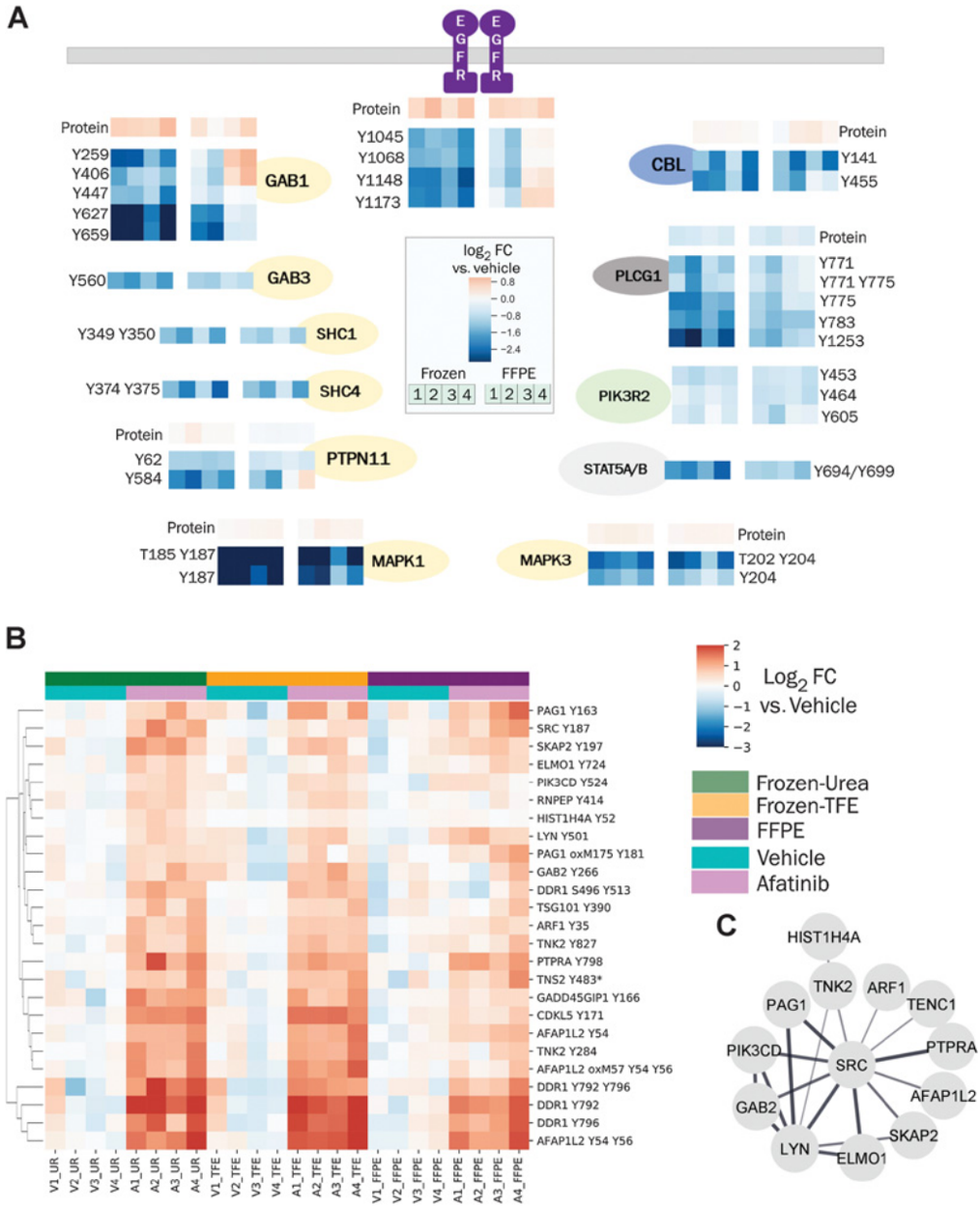

Figure 5.

Changes in pTyr and protein levels in response to afatinib treatment. **A,** Diagram of EGFR pathway showing the effect of afatinib treatment on selected pTyr sites in various proteins as quantified in Frozen-Urea and their FFPE counterparts. Protein or pTyr levels are represented as $\log_2$ fold change (FC) relative to vehicle control. **B,** Hierarchical clustering heatmap of pTyr sites that were significantly upregulated (fold change > 1.4 and FDR q-value < 0.05 after Benjamini–Hochberg multiple hypothesis testing correction) in response to afatinib treatment in Frozen-Urea workflow. Phosphotyrosine levels are represented as $\log_2$ fold change relative to vehicle control. Miscleaved peptides are denoted by * next to them. **C,** Interaction network of pTyr proteins from **B** obtained from STRING database. All of the interactions are at least medium confidence based on all interaction sources except text mining. Noninteracting proteins are not shown.

quantification of low-abundant posttranslational modifications such as pTyr requires additional enrichment and increased sensitivity. We developed a technique to quantify pTyr-regulated pathways to provide insight on tumor biology and inform on driving kinases. To the best of our knowledge, this is the first study to quantify tyrosine phosphorylation on several hundred proteins using one to two 10-µm sections of FFPE. In developing this method, the use of SP3 beads for sample processing and digestion provided an approximately 20-fold increase in sensitivity relative to previous publications (20, 41–44), enabling quantification of pTyr peptides from 50 µg of peptides from a single 10-µm FFPE section. Past studies have typically required >5 mg wet tissue, or 2.5×10^6 cells (assuming a cell volume of 2,000 μm^3) because of heavy losses during sample processing. Our method can provide robust quantitative information on hundreds of pTyr sites from just

50 μg of peptides or 1.25×10^5 cells, given the peptide yield of approximately 2 μg/mm^2 for a single 10-μm section. As pTyr signaling regulates many aspects of cell and tumor biology, the majority of the identified phosphoproteins belong to several well-characterized cancer pathways, highlighting that pTyr analysis can identify known actionable therapeutic targets from FFPE tissues.

The effects of FFPE preservation on pTyr signaling have not been previously characterized. By comparing the pTyr profiling in FFPE tissues and flash-frozen tissues derived from same tumor, we show that FFPE tissues can provide biologically relevant data compared with their flash-frozen pairs. While pTyr signaling was more affected by formalin fixing time relative to pSer/Thr or protein expression, the effects of afatinib treatment could still be determined from FFPE tissues. Comparison of pTyr levels between archived flash-frozen and FFPE tissues from patients with breast cancer further substantiated our findings from PDX analyses and highlighted that clinical FFPE tissues could provide similar information compared with their frozen counterparts. However, some caution has to be taken while interpreting the data from FFPE tissues alone because some changes associated with formalin fixation may alter physiologic signaling. We observed higher CV and poorer correlation among biological replicates in FFPE tissues compared with their frozen counterparts, suggesting some changes during fixation process. In addition, delays in freezing or formalin fixing after surgical resection can affect phosphorylation-mediated cell signaling networks, and thus uniform sample collection procedures are required in the clinic. However, sample collection procedures in hospital are estimated to have up to an hour delay before freezing or formalin fixing after surgery. The analysis of breast cancer clinical samples suggests that FFPE and tissues derived from same tumor can provide similar pTyr signaling, suggesting that the effects due to formalin fixation might be less significant compared with the effect of delayed processing (freezing or fixing) after resection. Immediate freezing or fixing of samples would lead to better preservation of activated signaling networks in clinical specimens. Thus, if possible, flash-frozen samples should be used to avoid any discrepancies arising from fixation process.

While flash freezing can preserve the signaling networks instantaneously (at the seconds timescale), formalin fixation has been reported to be much slower (at minutes-hours timescale) and dependent on tissue size (35). Some of the differences in pTyr signaling between flash-frozen and FFPE breast cancer tissues may be due to delays in fixing in larger tumors. A more controlled study looking at effect of tumor size on preservation of pTyr signaling in FFPE tissue is warranted, especially given that the PDX tumors were relatively small (200–250 mm^3), possibly leading to faster fixing than observed in the clinic for patient tumors. Separately, given the intratumor heterogeneity, a single 10-μm section may not represent the signaling state of the entire tumor. Additional sections from different parts of the tumor should be analyzed to get a comprehensive readout of pTyr signaling in the tumor.

Formalin fixing and paraffin embedding is a universal technique for tissue preservation following tissue biopsy and surgical resection, and thus FFPE tissues are readily available. Exome sequencing is commonly used to identify genetic alterations, and transcript profiling typically serves as a proxy for pathway activation. Although tyrosine phosphorylation consists of low-level signals, quantification of pTyr can provide translationally relevant information in identifying activated oncogenes in tumor samples. Here we highlight the capability of pTyr analysis of FFPE tissue sections as a method to directly measure signaling network activation in tumors. This approach is amenable to retrospective analysis of clinical specimens, and may be useful to highlight signaling networks associated with therapeutic response/resistance, or to freshly acquired tissues in the clinic for both patient stratification as well as assessing early response to therapeutic interventions.

Authors' Disclosures

I.N. Kohale reports grants from NIH during the conduct of the study. J. Kuang reports grants from NIH during the conduct of the study. J.C. Boughey reports grants from NIH and foundations during the conduct of the study, as well as grants from Lilly outside the submitted work. E.B. Haura reports grants from NCI during the conduct of the study; grants and personal fees from Revolution Medicines, personal fees and non-financial support from Janssen, and personal fees from Amgen outside the submitted work; and a patent for Protein–Protein Interactions as Cancer Biomarkers issued to Moffitt. M.P. Goetz reports other support from Eagle Pharmaceuticals, Lilly, Biovica, Novartis, Sermonix, Context Therapeutics, Pfizer, Biotheranostics, and AstraZeneca and grants from Pfizer, Sermonix, and Lilly outside the submitted work. J.N. Sarkaria reports grants from Basilea, GlaxoSmithKline, Bristol Myers Squibb, Curtana, Forma, AbbVie, Boehringer Ingelheim, Bayer, Celgene, Cible, Wayshine, Boston Scientific, AstraZeneca, Black Diamond, Karyopharm, and Actuate outside the submitted work. No disclosures were reported by the other authors.

Authors' Contributions

I.N. Kohale: Conceptualization, data curation, formal analysis, validation, investigation, visualization, methodology, writing–original draft, writing–review and editing. **D.M. Burgenske:** Conceptualization, investigation. **A.C. Mladek:** Investigation. **K.K. Bakken:** Investigation. **J. Kuang:** Investigation, methodology. **J.C. Boughey:** Conceptualization. **L. Wang:** Conceptualization. **J.M. Carter:** Investigation, writing–review and editing. **E.B. Haura:** Conceptualization, supervision. **M.P. Goetz:** Conceptualization, supervision. **J.N. Sarkaria:** Conceptualization, supervision. **F.M. White:** Conceptualization, resources, supervision, funding acquisition, writing–original draft, project administration, writing–review and editing.

Acknowledgments

The authors thank members of the White lab for helpful suggestions and the Koch Institute's Robert A. Swanson (1969) Biotechnology Center for technical support, specifically the Hope Babette Tang (1983) Histology Facility and the Biopolymers & Proteomics Core Facility. This research was supported by funding from MIT Center for Precision Cancer Medicine; NIH grants U54 CA210180, U01 CA238720, P42 ES027707, and P30 CA14051; and a Koch Institute - Mayo Clinic Cancer Solutions Team Grant. This research was funded in part by the Mayo Clinic Breast Cancer Specialized Program of Research Excellence Grant (P50CA 116201 to M.P. Goetz, J.M. Carter, and L. Wang) and the George M. Eisenberg Foundation for Charities (to M.P. Goetz, L. Wang, and J.C. Boughey).

The publication costs of this article were defrayed in part by the payment of publication fees. Therefore, and solely to indicate this fact, this article is hereby marked "advertisement" in accordance with 18 USC section 1734.

Note

Supplementary data for this article are available at Cancer Research Online (http://cancerres.aacrjournals.org/).

Received January 20, 2021; revised April 7, 2021; accepted May 6, 2021; published first May 20, 2021.

References

1. Letai A. Functional precision cancer medicine-moving beyond pure genomics. Nat Med 2017;23:1028–35.
2. Friedman AA, Letai A, Fisher DE, Flaherty KT. Precision medicine for cancer with next-generation functional diagnostics. Nat Rev Cancer 2015;15:747–56.
3. Rikova K, Guo A, Zeng Q, Possemato A, Yu J, Haack H, et al. Global survey of phosphotyrosine signaling identifies oncogenic kinases in lung cancer. Cell 2007;131:1190–203.
4. Hunter T, Sefton BM. Transforming gene product of Rous sarcoma virus phosphorylates tyrosine. Proc Natl Acad Sci U S A 1980;77:1311–5.

5. Olsen JV, Blagoev B, Gnad F, Macek B, Kumar C, Mortensen P, et al. Global, in vivo, and site-specific phosphorylation dynamics in signaling networks. Cell 2006;127:635–48.
6. Blume-Jensen P, Hunter T. Oncogenic kinase signalling. Nature 2001;411: 355–65.
7. Kannaiyan R, Mahadevan D. A comprehensive review of protein kinase inhibitors for cancer therapy. Expert Rev Anticancer Ther 2018;18:1249–70.
8. van Alphen C, Cloos J, Beekhof R, Cucchi DGJ, Piersma SR, Knol JC, et al. Phosphotyrosine-based phosphoproteomics for target identification and drug response prediction in AML cell lines. Mol Cell Proteomics 2020;19:884–99.
9. Lescarbeau RS, Lei L, Bakken KK, Sims PA, Sarkaria JN, Canoll P, et al. Quantitative phosphoproteomics reveals Wee1 kinase as a therapeutic target in a model of proneural glioblastoma. Mol Cancer Ther 2016;15:1332–43.
10. Grillo F, Bruzzone M, Pigozzi S, Prosapio S, Migliora P, Fiocca R, et al. Immunohistochemistry on old archival paraffin blocks: is there an expiry date? J Clin Pathol 2017;70:988–93.
11. Hughes CS, Moggridge S, Müller T, Sorensen PH, Morin GB, Krijgsveld J. Single-pot, solid-phase-enhanced sample preparation for proteomics experiments. Nat Protoc 2019;14:68–85.
12. Hughes CS, Mcconechy MK, Cochrane DR, Nazeran T, Karnezis AN, Huntsman DG, et al. Quantitative profiling of single formalin fixed tumour sections: proteomics for translational research. Sci Rep 2016;6:34949.
13. Eckert MA, Coscia F, Chryplewicz A, Chang JW, Hernandez KM, Pan S, et al. Proteomics reveals NNMT as a master metabolic regulator of cancer-associated fibroblasts. Nature 2019;569:723–8.
14. Coscia F, Doll S, Bech JM, Schweizer L, Mund A, Lengyel E, et al. A streamlined mass spectrometry–based proteomics workflow for large-scale FFPE tissue analysis. J Pathol 2020;251:100–12.
15. Gajadhar AS, Johnson H, Slebos RJC, Shaddox K, Wiles K, Washington MK, et al. Phosphotyrosine signaling analysis in human tumors is confounded by systemic ischemia-driven artifacts and intra-specimen heterogeneity. Cancer Res 2015;75: 1495–503.
16. Mertins P, Yang F, Liu T, Mani DR, Petyuk VA, Gillette MA, et al. Ischemia in tumors induces early and sustained phosphorylation changes in stress kinase pathways but does not affect global protein levels. Mol Cell Proteomics 2014;13: 1690–704.
17. Vaubel RA, Tian S, Remonde D, Schroeder MA, Mladek AC, Kitange GJ, et al. Genomic and phenotypic characterization of a broad panel of patient-derived xenografts reflects the diversity of glioblastoma. Clin Cancer Res 2020;26: 1094–104.
18. Bian Y, Li L, Dong M, Liu X, Kaneko T, Cheng K, et al. Ultra-deep tyrosine phosphoproteomics enabled by a phosphotyrosine superbinder. Nat Chem Biol 2016;12:959–66.
19. Mou Y, Zhou XX, Leung K, Martinko AJ, Yu JY, Chen W, et al. Engineering improved antiphosphotyrosine antibodies based on an immunoconvergent binding motif. J Am Chem Soc 2018;140:16615–24.
20. Dittmann A, Kennedy NJ, Soltero NL, Morshed N, Mana MD, Yilmaz ÖH, et al. High-fat diet in a mouse insulin-resistant model induces widespread rewiring of the phosphotyrosine signaling network. Mol Syst Biol 2019;15: e8849.
21. Taus T, Köcher T, Pichler P, Paschke C, Schmidt A, Henrich C, et al. Universal and confident phosphorylation site localization using phosphoRS. J Proteome Res 2011, 10:5354–62.
22. Nichols AM, White FM. Manual validation of peptide sequence and sites of tyrosine phosphorylation from MS/MS spectra. Methods Mol Biol 2009;492: 143–60.
23. Szklarczyk D, Gable AL, Lyon D, Junge A, Wyder S, Huerta-Cepas J, et al. STRING v11: protein-protein association networks with increased coverage, supporting functional discovery in genome-wide experimental datasets. Nucleic Acids Res 2018;47:D607–13.
24. Shannon P, Markiel A, Ozier O, Baliga NS, Wang JT, Ramage D, et al. Cytoscape: a software environment for integrated models of biomolecular interaction networks. Genome Res 200313:2498–504.
25. Mi H, Muruganujan A, Ebert D, Huang X, Thomas PD. PANTHER version 14: more genomes, a new PANTHER GO-slim and improvements in enrichment analysis tools. Nucleic Acids Res 2018;47:D419–26.
26. Eid S, Turk S, Volkamer A, Rippmann F, Fulle S. KinMap: a web-based tool for interactive navigation through human kinome data. BMC Bioinformatics; 2017; 18:16.
27. Subramanian A, Tamayo P, Mootha VK, Mukherjee S, Ebert BL, Gillette MA, et al. Gene set enrichment analysis: a knowledge-based approach for interpreting genome-wide expression profiles. Proc Natl Acad Sci U S A 2005;102:15545–50.
28. Perez-Riverol Y, Csordas A, Bai J, Bernal-Llinares M, Hewapathirana S, Kundu DJ, et al. The PRIDE database and related tools and resources in 2019: improving support for quantification data. Nucleic Acids Res 2019;47: D442–50.
29. Zhang Y, Wolf-Yadlin A, White FM. Quantitative proteomic analysis of phosphotyrosine-mediated cellular signaling networks. Methods Mol Biol 2007;359: 203–12.
30. Sarkaria JN, Yang L, Grogan PT, Kitange GJ, Carlson BL, Schroeder MA, et al. Identification of molecular characteristics correlated with glioblastoma sensitivity to EGFR kinase inhibition through use of an intracranial xenograft test panel. Mol Cancer Ther 2007;6:1167–74.
31. An Z, Aksoy O, Zheng T, Fan QW, Weiss WA. Epidermal growth factor receptor and EGFRvIII in glioblastoma: signaling pathways and targeted therapies. Oncogene 2018;37:1561–75.
32. Pearson JRD, Regad T. Targeting cellular pathways in glioblastoma multiforme. Signal Transduct Target Ther 2017;2:17040.
33. Fan QW, Weiss WA. Targeting the RTK-PI3K-mTOR axis in malignant glioma: overcoming resistance. Curr Top Microbiol Immunol 2010;347:279–96.
34. Smith MA, Hall R, Fisher K, Haake SM, Khalil F, Schabath MB, et al. Annotation of human cancers with EGFR signaling-associated protein complexes using proximity ligation assays. Sci Signal 2015;8:ra4.
35. Thavarajah R, Mudimbaimannar VK, Elizabeth J, Rao UK, Ranganathan K. Chemical and physical basics of routine formaldehyde fixation. J Oral Maxillofac Pathol 2012;16:400–5.
36. Hwang SY, Park S, Kwon Y. Recent therapeutic trends and promising targets in triple negative breast cancer. Pharmacol Ther 2019;199:30–57.
37. Johnson H, White FM. Quantitative analysis of signaling networks across differentially embedded tumors highlights interpatient heterogeneity in human glioblastoma. J Proteome Res 2014;13:4581–93.
38. Emdal KB, Dittmann A, Reddy RJ, Lescarbeau RS, Moores SL, Laquerre S, et al. Characterization of in vivo resistance to osimertinib and JNJ-61186372, an EGFR/Met bispecific antibody, reveals unique and consensus mechanisms of resistance. Mol Cancer Ther 2017;16:2572–85.
39. Labots M, van der Mijn JC, Beekhof R, Piersma SR, de Goeij-de Haas RR, Pham TV, et al. Phosphotyrosine-based-phosphoproteomics scaled-down to biopsy level for analysis of individual tumor biology and treatment selection. J Proteomics 2017;162:99–107.
40. Creelan BC, Gray JE, Tanvetyanon T, Chiappori AA, Yoshida T, Schell MJ, et al. Phase 1 trial of dasatinib combined with afatinib for epidermal growth factor receptor- (EGFR-) mutated lung cancer with acquired tyrosine kinase inhibitor (TKI) resistance. Br J Cancer 2019;120:791–6.
41. Chua XY, Mensah T, Aballo T, Mackintosh SG, Edmondson RD, Salomon AR. Tandem mass tag approach utilizing pervanadate BOOST channels delivers deeper quantitative characterization of the tyrosine phosphoproteome. Mol Cell Proteomics 2020;19:730–43.
42. Abe Y, Nagano M, Tada A, Adachi J, Tomonaga T. Deep phosphotyrosine proteomics by optimization of phosphotyrosine enrichment and MS/MS parameters. J Proteome Res 2017;16:1077–86.
43. Sathe G, Na CH, Renuse S, Madugundu A, Albert M, Moghekar A, et al. Phosphotyrosine profiling of human cerebrospinal fluid. Clin Proteomics 2018;15:29.
44. Randall EC, Emdal KB, Laramy JK, Kim M, Roos A, Calligaris D, et al. Integrated mapping of pharmacokinetics and pharmacodynamics in a patient-derived xenograft model of glioblastoma. Nat Commun 2018;9:4904.